Journal of Alloys and Compounds 874 (2021) 159968

Contents lists available at ScienceDirect

Journal of Alloys and Compounds

journal homepage: www.elsevier.com/locate/jalcom

Regularities of the property changes in the compounds $EuLnCuS_3$ (Ln = La-Lu)

Anna V. Ruseikina[a,*], Vladimir A. Chernyshev[b], Dmitriy A. Velikanov[c], Aleksandr S. Aleksandrovsky[c,d], Nikolay P. Shestakov[c], Maxim S. Molokeev[d], Maxim V. Grigoriev[a], Oleg V. Andreev[a], Alexander A. Garmonov[e], Alexey V. Matigorov[f,g], Ludmila V. Melnikova[h], Anatoliy A. Kislitsyn[e], Svetlana S. Volkova[a]

[a] Institute of Chemistry, University of Tyumen, Tyumen 625003, Russia
[b] Institute of Natural Sciences and Mathematics, Ural Federal University, Ekaterinburg 620002, Russia
[c] Kirensky Institute of Physics, Federal Research Center KSC SB RAS, Krasnoyarsk 660036, Russia
[d] Siberian Federal University, Krasnoyarsk 660079, Russia
[e] Institute of Physics and Technology, University of Tyumen, Tyumen 625003, Russia
[f] Engineering Centre of Composite Materials Based on Wolfram Compounds and Rare-earth Elements, University of Tyumen, Tyumen 625003, Russia
[g] Institute of Chemistry and Chemical Technology, Federal Research Center KSC SB RAS, Krasnoyarsk 660049, Russia
[h] University of Tyumen, Tyumen 625003, Russia

ARTICLE INFO

Article history:
Received 29 January 2021
Received in revised form 1 April 2021
Accepted 10 April 2021
Available online 16 April 2021

Keywords:
Inorganic materials
Ab initio calculations
Thermochemistry
Magnetic measurements
Microhardness
Lattice dynamics

ABSTRACT

This work contains the results of complex experimental research of the compounds $EuLnCuS_3$ (Ln = La-Lu) enhanced by the DFT calculations. It is aimed at the data replenishment with particular attention to the revelation of regularities in the property changes, in order to extend the potential applicability of the materials of the selected chemical class. The ab initio calculations of the fundamental vibrational modes of the crystal structures were in good agreement with experimental results. The wavenumbers and types of the modes were determined, and the degree of the ion participation in the modes was also estimated. The elastic properties of the compounds were calculated. The compounds were found out to be IR-transparent in the range of 4000–400 cm^{-1}. The estimated microhardness of the compounds is in the range of 2.68–3.60 GPa. According to the DSC data, the reversible polymorphous transitions were manifested in the compounds $EuLnCuS_3$ (Ln = Sm, Gd-Lu): for $EuSmCuS_3$ $T_{\alpha\leftrightarrow\beta}$ = 1437 K, $\Delta H_{\alpha\leftrightarrow\beta}$ = 7.0 kJ·mol^{-1}, $T_{\beta\leftrightarrow\gamma}$ = 1453 K, $\Delta H_{\beta\leftrightarrow\gamma}$ = 2.6 kJ·mol^{-1}; for $EuTbCuS_3$ $T_{\alpha\leftrightarrow\beta}$ = 1478 K, $\Delta H_{\alpha\leftrightarrow\beta}$ = 1.6 kJ·mol^{-1}, $T_{\beta\leftrightarrow\gamma}$ = 1516 K, $\Delta H_{\beta\leftrightarrow\gamma}$ = 0.9 kJ·mol^{-1}, $T_{\gamma\leftrightarrow\delta}$ = 1548 K, $\Delta H_{\gamma\leftrightarrow\delta}$ = 1.6 kJ·mol^{-1}; for $EuTmCuS_3$ $T_{\alpha\leftrightarrow\beta}$ = 1543 K, $T_{\beta\leftrightarrow\gamma}$ = 1593 K, $T_{\gamma\leftrightarrow\delta}$ = 1620 K; for $EuYbCuS_3$ $T_{\alpha\leftrightarrow\beta}$ = 1513 K, $T_{\beta\leftrightarrow\gamma}$ = 1564 K, $T_{\gamma\leftrightarrow\delta}$ = 1594 K; for $EuLuCuS_3$ $T_{\alpha\leftrightarrow\beta}$ = 1549 K, $T_{\beta\leftrightarrow\gamma}$ = 1601 K, $T_{\gamma\leftrightarrow\delta}$ = 1628 K. In the $EuLnCuS_3$ series, the transition into either ferro- or ferrimagnetic states occurred in the narrow temperature range from 2 to 5 K. The tetrad effect in the changes of incongruent melting temperature and microhardness conditioned on rLn^{3+} as well as influencing of phenomenon of crystallochemical contraction were observed. For delimiting between space groups *Cmcm* and *Pnma* in the compounds $ALnCuS_3$, the use of the tolerance factor $t' = IR(A)\cdot IR(C) + a\times IR(B)^2$ was verified.

1. Introduction

New compounds containing combination of *d*- and *f*-elements are of great interest to solid state chemistry and materials science due to their physical properties which make them prospective materials in the field of infra-red and non-linear optics [1–7]. Copper-containing chalcogenides are important multifunctional materials in such areas like photocatalysis, photovoltaics and proton conductivity [3,8–16]. They are prospective as thermoelectric materials with exceedingly low thermal conductivities [12]. They can be used in photoelectric equipment and as absorbers in solar cells [17–21] and in nonlinear optical devices [22–24]. Synthesis of new quaternary compounds of the type $A^{+2}B^{+3}Cu^{+1}(X^{-2})_3$ (A = *s*-, *p*- or *f*-element, B = *f*- or *d*-element, X = chalcogen) has been carried out for some decades [1,25–55]. Quaternary chalcogenides $ALnCuX_3$ exert a great variety of properties. Among them, there are

* Corresponding author.
E-mail address: a.v.rusejkina@utmn.ru (A.V. Ruseikina).

https://doi.org/10.1016/j.jallcom.2021.159968
0925-8388/

ferromagnetics [28,29], ferrimagnetics [28,30], paramagnetics [1] and diamagnetics [32]. The compounds are semiconductors with bandgap energy from 1.63 eV to 2.61 eV [1,12,26,40,42,44]. The europium-containing compounds possess narrower bandgap energy that is associated with the presence of *4f-5d*-transition in Eu^{2+} ion demonstrating ability to control bandgap energy of chalcogenides due to the embedded Eu [44]. $PbLaCuS_3$ possesses the conductivity of *p*-type with the projected bandgap energy ≈1.5 eV [32]. The quaternary chalcogenides are of various melting types like congruent [52–55] and incongruent [26,30,44,49,56,57] ones. The phase equilibria in multicomponent systems Cu_2X–AX–B_2X_3 [49–55,58–60] have complex nature, including peritectic, eutectic, eutectoid, peritectoid interactions and formation of extensive solid solution areas.

The compounds $ALnCuS_3$ (A = Sr, Ba, Eu, Pb) crystallize in four structural types of the orthorhombic system [26–28,30–33,40–42, 44,45,49,50,53,57,61–71]; see this table SI in Supplementary Information for more detail.

Sulfides $EuLnCuS_3$ (Ln = La-Nd, Gd, Dy-Er) melt incongruently and three polymorphous transitions in the temperature range of 1400–1610 K were detected for some of them [30,57,58]. The transition into the ordered magnetic state for $EuLnCuS_3$ (Ln = Y, Eu, Tb, Dy, Er-Lu) compounds occurs in the narrow temperature range from 3.4 to 5.5 K [28–30].

Despite the fact that the structure of the compounds $EuLnCuS_3$ (Ln = La-Lu) was actually solved and refined previously, the data concerning their properties and physicochemical characteristics are still incomplete. This restricts the potentialities of their practical use.

The aim of this work is a comprehensive study of the compounds $EuLnCuS_3$ (Ln = La-Lu), in particular, the experimental determination of thermal, optical, magnetic, durometric properties, the performance of ab initio calculations of crystal structures, phonon spectra, elastic properties, and the determination of regularities in their property changes depending on rLn^{3+}.

2. Materials and methods

2.1. Materials

The rare-earth element oxides Ln_2O_3 (Ln = La, Nd, Sm, Gd, Dy-Lu), LnO_2 (Ln = Ce, Pr) and Tb_4O_7 (99.9%) were procured at the manufacture of Uralredmet (Russia). Elementary sulfur (99.99%) was purchased in the Komponent-reactive manufacture (Russia). Elementary copper (99.99%) was procured in Red Chemist, Ltd. (Russia). Argon (99.998%) was purchased from the technical gases manufacture Kislorod-servis (Russia). Epoxy glue was procured in OOO Scientific-Industrial Complex “Astat” (Russia). GOI polishing paste was purchased in OOO “Tehnopayka” (Russia).

2.2. Methods

The compounds $EuLnCuS_3$ were synthesized by melting the intermediate sulfides mixed in the ratio 2EuS: $1Ln_2S_3$: $1Cu_2S$. The compound Cu_2S was prepared from Cu and S by the ampoule method according to the technique described earlier [49]. The compounds EuS, Ln_2S_3 were synthesized at 1300 K from the rare-earth element oxides in the flow of H_2S and CS_2, produced by decomposition of ammonium rhodanide (the carrier gas is argon) [30]. The powdered batch composed of 2EuS: $1Ln_2S_3$:$1Cu_2S$ was molten in the argon atmosphere in a graphite crucible placed in the silica reactor. The synthesized samples were annealed in evacuated and sealed-off silica glass ampoules at 1170 K for 1500 h [63]. No interaction of the samples with silica was found during annealing.

The X-ray diffraction measurements were performed by means of an X-ray diffractometer PANalytical X'Pert PRO equipped with the detector PIXcel (Co Kα-emission, graphite monochromator) and DRON 7 (CuKα-emission and Ni filter) at 298 K. The X-ray diffraction patterns were scanned at 298 K over the diffraction angles $10^o \le 2\theta \le 125(140)^o$ in the increments of 0.013° and total accumulation time 13 h. The crystal structures of the whole series of $EuLnCuS_3$ were previously refined in terms of the powder data by the derivative difference minimization method (DDM) and Rietveld method [28,44,63], and the X-ray analysis was performed to determine chemical composition and the phase purity of the synthesized samples, that is important for the measurements of thermal, optical and magnetic properties. According to the X-ray diffraction analysis, the structural type of the compounds and the unit cell parameters were consistent with the earlier data [28,44,63].

The microstructure was observed on polished samples using the AxioVert.A1 and Olympus GX-71 microscopes. Scanning electron microscopy (SEM) was performed on a Philips SEM 515 and JEOLJSM-6510 LV equipped with an energy dispersive spectrometer.

The differential scanning calorimetry experiments were carried out on a Setsys Evolution 1750 (TG–DSC 1600) with the aid of the PtRh 6%-PtRh 30% thermocouple. The complex was calibrated according to the data of melting temperatures and melting enthalpies of standard substances (Sn, Pb, Zn, Al, Ag, Au, Cu, and Pd). Prior to an experiment, the working chamber of the complex was evacuated and then filled with argon. The recording parameters were the following: the sample size: 100–110 mg, heating rate: 5 K/min, argon flow rate: 25 ml/min, and alundum crucible capacity: 100 µl. The heat absorption onset temperature was determined as the intersection point of a tangent with the baseline in the program package Setsoft Software 2000 with a linear baseline from the first to last point. The temperatures and enthalpies of the thermal events appearing in replica measurements were aligned with the thermoanalytical error bar. While performing thermal analysis up to 1840 K, the samples transformed into melt. The TG curves showed a 0.16 wt% weight loss in the samples of $EuLnCuS_3$ (Ln = Tb, Tm, Yb, Lu).

The graphical plottings were acquired by means of the program Edstate 2d [72]. The crystal structures were visualized in the software package Diamond 3 [73].

Durometric analysis of a polished sample was performed by the Vickers method on an HMV-G21 [74]. The samples were used in the cylindrical form and poured over with epoxy glue (EP resin and solidifier in the ratio 100:12). Then, they were smoothed, and finally polished by GOI polishing paste. The exposure time was 15 s and the load was 10 kg-force (98.07 N).

The low-temperature (1.8–50 K) magnetic susceptibilities of $EuLnCuS_3$ (Ln = La, Ce, Pr, Nd, Sm, Ho) were studied on a SQUID magnetometer [75–77] in a 10 Oe magnetic field. Masses of the samples were 0.0862 g ($EuLaCuS_3$), 0.0475 g ($EuCeCuS_3$), 0.1025 g ($EuPrCuS_3$), 0.0655 g ($EuNdCuS_3$), 0.1055 g ($EuSmCuS_3$), 0.0786 g ($EuHoCuS_3$).

The dilatometric analysis was performed by means of a DIL 402 PC in the following conditions: the temperature range for measurements was 300–1240 K, heating rate was 5 K/min, pressure of the puller contact was 30 cH, purge speed of argon was 25 ml/min. The measurements were performed on the tablet with the diameter of 6 mm and 1.28–3.3 mm thick. The initial length L_0 of the samples was determined with the absolute error ± $5 \cdot 10^{-3}$ mm, while percentage error of the initial length measurement is within the range of 0.15–0.4%. The percentage error of the measurements of elongation ΔL during the thermal dilatation process was 5%, and the percentage error $\Delta L/L_0$ ranged from 5.15% to 5.4%. The dependencies of the relative elongation of the samples on the temperature were

Table 1
Lattice constants of $EuLnCuS_3$ (Å).

Compound	S.G.	ST	*a*	*b*	*c*	*Volume*	a/c	
							Calc.	Exp.
$EuPrCuS_3$	*Pnma*	Ba_2MnS_3	7.9854	4.0540	15.7090	509	0.5083	0.5100 [63]
$EuSmCuS_3$	*Pnma*	Eu_2CuS_3	10.4978	4.0114	12.7145	535	0.8257	0.8134 [63]
$EuGdCuS_3$	*Pnma*		10.3755	3.9901	12.7571	528	0.8133	0.8041 [28]
$EuTbCuS_3$	*Pnma*		10.3158	3.9801	12.7742	524	0.8075	0.7985 [28]
$EuDyCuS_3$	*Pnma*		10.2579	3.9714	12.7908	521	0.8020	0.7932 [28]
$EuHoCuS_3$	*Pnma*		10.2005	3.9633	12.8014	518	0.7968	0.7898 [57]
$EuYCuS_3$	*Pnma*		10.0590	3.9233	12.8996	509	0.7798	0.7925 [28]
$EuErCuS_3$	*Pnma*		10.1501	3.9544	12.8261	515	0.7914	0.7862 [30]
$EuTmCuS_3$	*Cmcm*	$KZrCuS_3$	3.9477	12.8220	10.1150	512	0.3903	0.3889 [28]
$EuYbCuS_3$	*Cmcm*		3.9407	12.8174	10.0809	509	0.3909	0.3895 [28]
$EuLuCuS_3$	*Cmcm*		3.9337	12.8562	10.0403	508	0.3918	0.3898 [28]

approximated by some linear functions by the procedure described in [78]. The approximation data were assessed by Fisher's ratio test: $F = \frac{S_0}{S}$, $S_0 = \frac{1}{N-1}\sum_{i=1}^{N}(y_{iexp-}\langle y_{iexp}\rangle)^2$ – the total variance, $S = \frac{1}{N-1}\sum_{i=1}^{N}(y_{iexp-}\langle y_{iappr}\rangle)^2$ – the remainder variance [78]. We selected both the values of the temperature range limits and the $\alpha(T)$ values, wherein the minimal values of the remainder variance conformed the determined polynomials.

The infrared absorption spectra were recorded in the range of 680–85 cm^{-1} using an FTIR VERTEX 80 V spectrometer (BRUKER OPTIK GMBH) equipped by an RT-DTGS FIR sensor. The sulfide powders under investigation were grinded in agate mortar and then mixed with ultrahigh molecular weight polyethylene (Mitsui Petrochemical Ind., Japan) in a ratio 1:10 and pressed into 0.26 mm thick pellets.

The IR spectra of the compounds $EuLnCuS_3$ were recorded in the range of 4000–400 cm^{-1} using a FTIR spectrometer. The polycrystalline sample was grinded in agate mortar and mixed with the annealed potassium bromide powder to get a homogeneous mix, and then pressed into a pellet in the mold PF13 using an automatic hydraulic press Autotouch 9t. The pressure resistance time was 2 min

The crystal structure, phonon spectrum, and elastic properties of the $EuLnCuS_3$ compounds were investigated at ab initio level of theory. The calculations were carried out in the framework of density functional theory (DFT) [79] by using the B3LYP hybrid functional [80,81], which takes into account both local and nonlocal Hartree-Fock exchanges. The functional allows to successfully describe complex compounds with an ionic-covalent bond [82,83]. The calculations were performed in the CRYSTAL17 program designed to simulate periodic structures [84,85]. The sequence of calculations was as follows. First, the optimization of the crystal structure was carried out. After that, the phonon spectrum (at the Γ- point) or elastic constants were calculated for the crystal structure corresponding to the minimum energy.

For europium, the ECP53MWB quasi-relativistic pseudo-potential [86,87] was used with the attached valence basis set ECP53MWB [88]. The Gaussian primitives with exponents less than 0.1 were removed from the basis sets. The exponent in the outer *d*- orbital of the valence basis set was set to 0.178. For copper, the full-electron basis set [89] was used, as available on the CRYSTAL program site as "Cu_86–4111(41D)G_doll_2000" [49]. For sulfur, the DURAND pseudo-potential with the attached valence basis set was used [49,90]. The exponents in the two outer orbitals of the valence basis set were set to 0.20 and 0.22. The quasi-relativistic pseudopotentials ECP*n*MWB were used to describe the inner shells of rare-earth ions (*n* is the number of internal electrons replaced by the pseudopotential) [91,92]. For La *n* = 46, for Ce *n* = 47, etc. Thus, the inner shells of the rare-earth ion, 4*f* including, were replaced by a pseudopotential. To describe the outer shells $5s^25p^6$ involved in chemical bond, the valence basis sets "ECP*n*MWB-II" [91–94] were used. The Gaussian primitives with orbital exponent values less than 0.1 were removed from the valence basis set, since these calculations are periodic. We used pseudo-potentials for the description of core electronic shells of rare-earth ions, the 4*f* inclusive, with the valence basic sets for outer orbitals involved in chemical bonding. Such approach makes it possible to reconstitute successfully both the lattice structure and dynamics in the compounds that have a lanthanide ion sublattice [95,96].

The accuracy of calculating the self-consistent field was set at 10^{-9} a.u. The accuracy of the calculation of the two-electron integrals was set at least 10^{-8}. Integration over the Brillouin zone was carried out according to the Monkhorst-Pack scheme with a grid of k-points equal to 8 × 8 × 8. The details of the calculation algorithm were considered previously [95]. The calculations were done for all stoichiometric compounds $EuLnCuS_3$ (Ln = Sm-Lu and Y). The modeling of non-stoichiometric compounds requires an increase of the unit cell and high computer costs. Therefore, the modeling of non-stoichiometric compounds $EuLnCuS_3$ (Ln = La, Ce, Pr, Nd) was not carried out. For the crystal $EuPrCuS_3$, the calculations were done in the stoichiometric approximation.

3. Results and discussion

3.1. The ab initio calculations of the $EuLnCuS_3$ crystal structure

The structure of the compounds $EuLnCuS_3$ (Ln = La-Lu) was actually solved and refined previously [28,29,44,63]. The calculated lattice constants in comparison with the experimental data are given in Table 1. The ratio *a/c* obtained from the calculation for the crystals $EuLnCuS_3$ is consistent with experimental data [28,30,57,63].

For the detailed observation, we synthesized the series of the compounds $EuLnCuS_3$. The photos of obtained samples can be seen in Fig. S1. Powdered compounds $EuLnCuS_3$ consist of planar particles with linear sizes up to 20 μm (Fig. S2). The energy dispersive X-ray spectrometric analysis was performed at 5 different locations on the surface of each sample. The chemical compositions of the samples were consistent with the theoretical contents of the elements (Table 2) and with the XRD analysis data, presented earlier [28,44,63].

In series of the compounds $EuLnCuS_3$ (Ln = La - Lu), we can clearly observe two regularities, they are periodicity and continuity. The periodicity manifests itself in some changes of the ST compounds, particularly in the segments of crystallochemical instability (Table S1), namely, the types of polyhedra cations. While transmitting from ST Ba_2MnS_3 to ST Eu_2CuS_3, the LnS_7 one-capped trigonal prism is transformed into the LnS_6 octahedron (Fig. S3). In the segment of transition of ST Eu_2CuS_3 to ST $KZrCuS_3$, the coordination polyhedron of europium with one-cap trigonal prism CN = 7 is

Table 2
Elemental distribution over the surface of $EuLnCuS_3$ samples as probed by X-ray spectral microanalysis.

Compound	Eu		Ln		Cu		S	
	m_{calcd}	m_{found}	m_{calcd}	m_{found}	m_{calcd}	m_{found}	m_{calcd}	m_{found}
$EuSmCuS_3$	32.89	32.81	32.55	32.50	13.75	13.80	20.81	20.89
$EuTmCuS_3$	31.62	31.56	35.15	35.08	13.22	13.25	20.01	20.11
$EuYbCuS_3$	31.35	31.41	35.70	35.63	13.11	13.08	19.84	19.88
$EuLuCuS_3$	31.23	31.30	35.95	35.88	13.06	13.03	19.76	19.79

m_{calcd} and m_{found} are, respectively, the calculated mass percentage and the analyzed mass percentage of elements in $EuLnCuS_3$.

transformed into trigonal prism CN = 6. The changes of CN and coordination polyhedra must cause discontinuities in all the composition-property dependencies in a number of the rare-earth compounds $EuLnCuS_3$. The continuous functions will manifest themselves in monotonous changes of the unit cells parameters, phase microhardness, phase transition temperature in dependence on rLn^{3+} in a number of similar ST compounds.

3.2. Microhardness and elastic constants of crystals $EuLnCuS_3$

The microhardness values of the compounds $EuLnCuS_3$ regularly increase as rLn^{3+} reduced within the limits of each structural type (Fig. 1, Table 3). The type of the dependencies is consistent with the structural changes of the compounds. In the limits of ST Ba_2MnS_3, a slight change of microhardness was detected, if compared to the compounds of the two other types. The structures of Eu_2CuS_3 and $KZrCuS_3$-type are described as 2D layers located in planes *ab* and *ac*, respectively, with the Eu^{2+} ions positioned between the layers. Since the two-dimensional $[LnCuS_3]$ layers are formed by the distorted LnS_6 octahedra and CuS_4 tetrahedra, the decrease in the radius of the rare-earth ion leads to the crystallochemical contraction of the two-dimensional layers. This contraction is manifested in the decrease of the average Ln–S bond length, the changes in the unit cell parameters, and alteration of the local geometry around the Eu atom, as

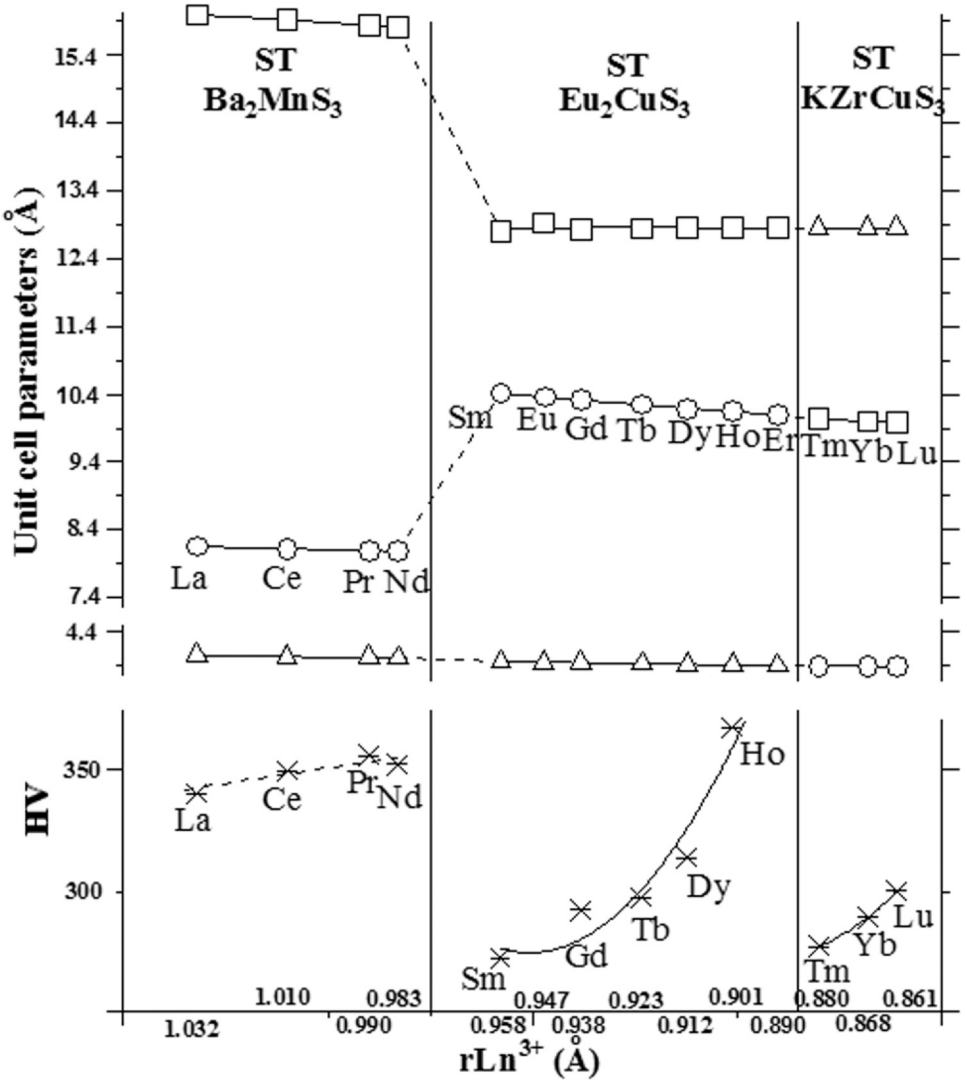

Fig. 1. Dependencies of the unit cell parameters (Å): ○ – *a*, Δ – *b*, □ – *c* and × – the compounds $EuLnCuS_3$ (microhardness values obtained in this research) on the radii of the rare-earth ion rLn^{3+}.

Table 3
Microhardness and color of the compounds $EuLnCuS_3$ (Ln = La-Lu).

Compound	H_V, GPa		Color	Compound	H_V, GPa		Color
	Exp.	Calc.			Exp.	Calc.	
$EuLaCuS_3$	3.33 ± 0.14	–	black	$EuDyCuS_3$	3.08 ± 0.25	3.95	brown
$EuCeCuS_3$	3.42 ± 0.26	–	black	$EuHoCuS_3$	3.60 ± 24	3.93	brown
$EuPrCuS_3$	3.49 ± 0.17	4.63	black	$EuYCuS_3$	–	3.83	–
$EuNdCuS_3$	3.45 ± 0.23	–	black	$EuErCuS_3$	2.85 [30]	3.83	Red-brown
$EuSmCuS_3$	2.68 ± 0.08	4.37	brown	$EuTmCuS_3$	2.73 ± 0.03	3.87	Red-brown
$EuGdCuS_3$	2.87 ± 0.21	4.30	brown	$EuYbCuS_3$	2.84 ± 0.21	3.99	brown
$EuTbCuS_3$	2.92 ± 0.23	4.15	brown	$EuLuCuS_3$	2.94 ± 0.22	4.17	Red-brown

Table 4
Temperatures (K) and enthalpies ($kJ \cdot mol^{-1}$) of the phase transitions in $EuLnCuS_3$ (Ln = La-Lu).

Compound	α↔β		β ↔ γ		γ↔δ		T_m or T_{cr}[a]	ΔH_{cr}[a] or ΔH_m
	T	ΔH	T	ΔH	T	ΔH		
$EuLaCuS_3$ [59]	–	–	–	–	–	–	1539 ± 4	23.3 ± 2.3
$EuCeCuS_3$ [98]	–	–	–	–	–	–	1524 ± 3	23.7 ± 2.3
$EuPrCuS_3$ [98]	–	–	–	–	–	–	1497 ± 3	20.1 ± 2.0
$EuNdCuS_3$ [60]	–	–	–	–	–	–	1470 ± 4	17.7 ± 1.8
$EuSmCuS_3$	1437 ± 4	7.0 ± 0.7	1453 ± 5	2.6 ± 0.3	–	–	1574 ± 8	4.2 ± 0.4
$EuGdCuS_3$ [99]	1460 ± 3	2.6 ± 0.3	1492 ± 5	2.3 ± 0.3	1525 ± 9	4.4 ± 0.4	1720 ± 5	-3.8 ± 0.4[a]
$EuTbCuS_3$	1478 ± 5	1.6 ± 0.2	1516 ± 3	0.9 ± 0.1	1548 ± 4	1.6 ± 0.2	1718 ± 6[a]	-3.3 ± 0.3[a]
$EuDyCuS_3$ [58]	1500 ± 6	4.4 ± 0.5	1543 ± 4	1.0 ± 0.1	1568 ± 6	2.0 ± 0.2	1727 ± 7	-4.6 ± 0.4[a]
$EuHoCuS_3$ [57]	1516 ± 1	3.7 ± 0.4	1562 ± 2	1.2 ± 0.1	1591 ± 2	2.2 ± 0.2	1737 ± 7[a]	-7.8 ± 0.8[a]
$EuErCuS_3$ [30]	1524 ± 2	2.3 ± 0.2	1575 ± 3	0.7 ± 0.1	1602 ± 3	1.3 ± 0.1	1735 ± 10[a]	-3.5 ± 0.3[a]
$EuTmCuS_3$	1543 ± 8	5.3 ± 0.5	1593 ± 7	1.3 ± 0.1	1620 ± 5	2.4 ± 0.2	1719 ± 6[a]	-8.6 ± 0.8[a]
$EuYbCuS_3$	1513 ± 10	2.3 ± 0.2	1564 ± 7	1.4 ± 0.1	1594 ± 8	2.4 ± 0.2	1732 ± 6[a]	-6.1 ± 0.6[a]
$EuLuCuS_3$	1549 ± 3	5.3 ± 0.5	1601 ± 2	1.5 ± 0.2	1628 ± 2	2.4 ± 0.2	1735 ± 6[a]	-8.8 ± 0.8[a]

[a] The data are based on the cooling curves.

well as the changes in the structure type and the space group. The manifestation of the effect of the crystallochemical contraction of two-dimensional layers is fully consistent with the increase of microhardness, also manifested in the isostructural compounds ($SrSmCuS_3$ 2.7 GPa, $SrErCuS_3$ 3.2 GPa [49]). Periodicity in the microhardness change as a function of rLn^{3+} confirms the manifestation of tetrad effect in series of complex sulfides $EuLnCuS_3$.

Since experimental data on elastic constants are absent in research papers, elastic constants of crystals $EuLnCuS_3$ were also calculated (Table S2). According to the calculations, the elastic constants of crystals with a structural type of Eu_2CuS_3 (*Pnma*) differ significantly from the elastic constants of crystals with a structural type of $KZrCuS_3$ (*Cmcm*) (Table S2). The column "Δ" in Table S2 shows the difference between the values of the elastic constants in structures Eu_2CuS_3 (*Pnma*) and $KZrCuS_3$ (*Cmcm*). (The average values were calculated for the series Sm-Er and Tm, Yb, Lu, respectively.) The values of C_{44} and C_{55} change several times. It is notable that the bulk modulus of compounds with structure Eu_2CuS_3 (*Pnma*) differs little from the bulk modulus of compounds with structure $KZrCuS_3$ (*Cmcm*). The calculated bulk modulus, Young modulus and shear modulus in the Voigt, Reuss and Hill approximations for $EuLnCuS_3$ are given in Table S3. The dependence of Young modulus on the crystallographic direction shows the anisotropy of elastic properties (Fig. S4).

The calculated values of the shear modulus and bulk modulus make it possible to estimate the Vickers hardness for $EuLnCuS_3$. To estimate the Vickers hardness, the known empirical formula (3.1) was used [97]. This formula well describes the hardness in the series of compounds with ionic and covalent types of chemical bond (about 40 compounds were considered in [97]).

$$H_V = 0.92\left(\frac{G}{B}\right)^{1.137} G^{0.708} \quad (3.1)$$

In (3.1), G and B are the bulk modulus and shear modulus by Hill estimation, respectively. As it was shown in [97], formula (3.1) provides good agreement with experimental values when hardness is larger than 5 GPa, but gives overestimated values at lower hardness. The experimental values of hardness are in the range of 2.7–3.6 GPa (Table 3). The formula (3.1) overestimates the hardness of $EuLnCuS_3$ by approx. 30% and does not describe the trend in the series La-Lu.

3.3. Thermal Properties

All the compounds melt incongruently to form polycrystalline phase EuS and the melt. According to the XRD and SEM data, the single-phase samples of the compounds $EuLnCuS_3$, crystallized from the melt during DSC were found to change into the three-phase samples. The microstructure of the samples contained primary crystals of the EuS phase, surrounded by the $EuLnCuS_3$ phase crystals. In the samples the eutectic consisting of the grains of the $EuLnCuS_3$ and $CuLnS_2$ phases was observed between the grains of the $EuLnCuS_3$ phase [58–60].

On the thermal curve of the compounds $EuLnCuS_3$ (Ln = Tb, Tm, Yb, Lu) the overlapping of endothermal melting effects of $EuLnCuS_3$ and the primary crystals of EuS is observed (Fig. S5). On the cooling curves, the thermal effects of the phase crystallization vary in temperatures and overlap to a lesser extent. Therefore, the temperature and enthalpy of incongruent melting were determined from the cooling curve.

The temperature data of this phase transition are given approximately, as the supercooling effect is observed. The exothermal effect of the crystallization process (ΔH = −24.8 J/g, e.g., for the compound $EuLuCuS_3$) was separated into two peaks (ΔH = −6.6 J/g and ΔH = −18.2 J/g). The first thermal effect manifested in the interval 1740–1735 K characterizes the formation of primary crystals EuS (ΔH = −1.2 kJ/mol), and the second one results from the interaction of primary crystals EuS with liquid to form the compound $EuLuCuS_3$ (ΔH = −8.8 kJ/mol). The analogous separation was carried out for $EuLnCuS_3$ (Ln = Tb, Tm, Yb) (Table 4).

While performing DSC measurements of the initial single-phased annealed samples of $EuLnCuS_3$, the phase transition peaks were

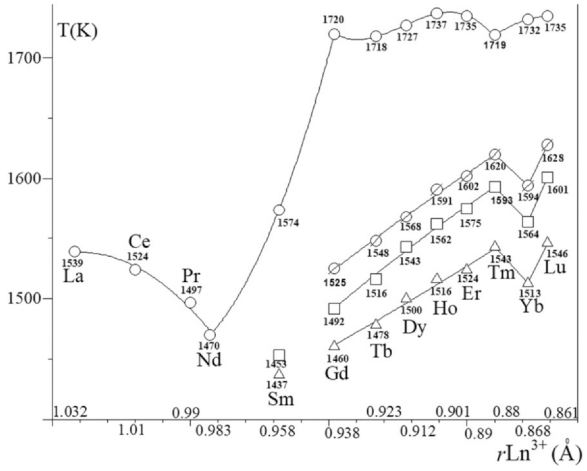

Fig. 2. Phase-transition temperatures of $EuLnCuS_3$ (Ln = La-Nd [98], Gd [99], Dy [58], Ho [57], for the Sm, Tb, Tm, Yb and Lu compounds the phase transition temperatures were measured in this work): Δ $\alpha \rightarrow \beta$; □ $\beta \rightarrow \gamma$; and Ø $\gamma \rightarrow \beta$ polymorphic transitions and ○ incongruent melting.

detected for the first time. The compounds $EuLnCuS_3$ were subdivided into three groups for the rare-earth elements La-Nd, Sm and Gd-Lu according to the number of the phase transitions.

For the compounds $EuLnCuS_3$ (Ln = La, Ce, Pr, Nd), the polymorphous transitions were not detected by the DSC method. The decrease of the incongruent melting temperatures of complex sulfides $EuLnCuS_3$ (Ln = La-Nd) and enthalpies of their melting indicates lowering of thermodynamic stability of these compounds (Fig. 2).

The compound $EuSmCuS_3$ was classified into a separate group since two polymorphous transitions resulted in thermal stability improvement were found out.

In the compounds $EuLnCuS_3$ (Ln = Gd-Lu), three endoeffects (Fig. 6, Table 4) reproduced in cooling of the samples were detected on the heating curves in the temperature range of 1430–1640 K. Within this temperature range, after the third endoeffect, the samples remain in polycrystalline state. The thermal effects defined in $EuLnCuS_3$ (Ln = Sm, Gd-Lu) resulted from the phase changes of the first type, i.e. polymorphous transitions. Similar transitions were earlier detected in isostructural compounds $SrLnCuS_3$ [56]. The polymorphous transitions are designated by Greek letters in the order of increasing temperatures. Temperatures and enthalpies of the phase transitions are determined according to heating curves and they are presented in Table 4. The phase transitions proceed in temperature interval up to 10 K. We were not succeeded in producing high temperature modifications of the compounds $EuLnCuS_3$ by quenching into a coolant liquid since the polymorphous transitions are classified as rapid ones and they can be detected by kinetic method.

In the series of compounds $EuSmCuS_3$-$EuLuCuS_3$, the temperatures of polymorphous transitions increase monotonously as a function of rLn^{3+}. The presence of local minimum for the compound $EuYbCuS_3$ correlates to 4*f*-electronic level occupation in Yb atom.

In the series of the compounds, two general regularities, such as lowering of thermodynamic stability of the compounds for REEs La-Nd and polymorphism and thermal stability improvement for REEs Gd – Lu, were shown up. The abrupt changes of physicochemical properties of the compounds $EuLnCuS_3$ are the most likely caused by the changes in the nature of the compounds as sulfide salts.

The compounds $EuLnCuS_3$ are formed by basic sulfide EuS and sulfides Cu_2S and Ln_2S_3 exerting acidic properties in relation to EuS sulfide. Acidity of sesquisulfides of rare-earth elements increases in consequence of both rLn^{3+} reduction [71] and the increase of electronegativity of rare-earth atoms (XSm = 1.37; XTb = 1.40; XEr = 1.47; XTm=1.48 [100]). Such increasing of Ln_2S_3 acidity affects the acid-base nature of complex sulfides $EuLnCuS_3$.

In series of the compounds $EuLnCuS_3$, in the segment from Nd to Sm, we observed the transformation of the structural type Ba_2MnS_3, being typical for the sulfide $EuNdCuS_3$, into the structural type Eu_2CuS_3, which is intrinsic to $EuSmCuS_3$. The coordinal polyhedron of lanthanide cation is transformed from one-cap trigonal prism NdS_7 into octahedron SmS_6. In the segment Nd–Sm–Gd, thermal stability of the compounds $EuLnCuS_3$ remarkably increases (Fig. 7).

The compounds $EuLnCuS_3$ (Ln = La-Nd) are classified as thiocuprates because acidity of Cu_2S dominates over the Ln_2S_3 acidity. With increase of acidity of Ln_2S_3 in series from La to Nd, the temperature of incongruent melting of $EuLnCuS_3$ decreases appropriately. The compounds $EuLnCuS_3$ (Ln = Sm-Lu) belong to thiolanthanate group as in series of these compounds both polymorphous transition temperatures and their thermal stability increases.

According to the DSC data for the compounds $EuLnCuS_3$ the phenomenon of polymorphism, character of the compound melting, regularities of the thermal characteristic changes of the phase transitions in the series of compounds were determined.

3.4. Magnetic properties

The temperature dependence of the inverse magnetic susceptibility of the compounds $EuLnCuS_3$ for Ln = La, Ce, Pr, Nd, Sm corresponds to Curie-Weiss law that allows to classify these compounds to ferromagnetics (Fig. S6). The calculated and experimental Curie constants are in satisfactorily relation (Table 5). The Curie-Weiss parameters Θ_W were calculated and the values are listed in Table 5.

The dependence of inverse magnetic susceptibility on temperature in $EuHoCuS_3$ is approximated by Neel's relation for ferrimagnetics:

$$\frac{1}{\chi} = \frac{T}{C} + \frac{1}{\chi_0} - \frac{\sigma}{T - \theta} \tag{3.2}$$

The calculated parameters of the model are the following: $C = 0.217$ K·m^3/kmol, $1/\chi_0 = 0.243$ kmol/m^3, $\sigma = 12.2$ kmol·K/m^3, $\theta = 4.30$ K. Curie point calculated from these parameters according to the formula

$$T_c = \frac{1}{2}\left(\theta - \frac{C}{\chi_0} + \sqrt{\left(\theta - \frac{C}{\chi_0}\right)^2 + 4C\left(\frac{\theta}{\chi_0} + \sigma\right)}\right), \tag{3.3}$$

is equal to 4.8 K.

The study of magnetic properties of the compounds $EuLnCuS_3$ (Fig. S6, Table 5) allows to determine common regularities of their

Table 5
The calculated and experimentally determined Curie constants (C), Curie-Weiss parameters (Θ_W), maximum inverse magnetic susceptibility temperature (T_{max}), and the arrangement type (F - ferromagnetic; Fe - ferrimagnetic).

Characteristics	$EuLaCuS_3$	$EuCeCuS_3$	$EuPrCuS_3$	$EuNdCuS_3$	$EuSmCuS_3$	$EuHoCuS_3$
C_{theor} (K·m^3/kmol)	0.0990	0.109	0.119	0.120	0.100	0.276
C_{exp} (K·m^3/kmol)	0.0991	0.104	0.118	0.120	0.0994	0.228
Θ_W, K	3.6	4.8	0.5	3.2	5.3	–
T_{max}, K	2.4	2.7	2.1	3.1	3.1	4.8
Arrangement type	F	F	F	F	F	Fe

Table 6
Magnetic moment of the Ln^{3+} ion in $EuLnCuS_3$ and type of magnetic ordering.

Ion	M_{theor}, μ_B	Arrangement	Ion	M_{theor}, μ_B	Arrangement
La^{3+}	0	F	Tb^{3+}	9.72	Fe [28]
Ce^{3+}	2.54	F	Dy^{3+}	10.63	Fe [28]
Pr^{3+}	3.58	F	Ho^{3+}	10.60	Fe
Nd^{3+}	3.62	F	Er^{3+}	9.59	Fe [30]
Pm^{3+}	2.68	No data	Tm^{3+}	7.57	Fe [28]
Sm^{3+}	0.84	F	Yb^{3+}	4.54	F [28]
Gd^{3+}	7.94	Fe [28]	Lu^{3+}	0	F [28]

changes in series of REEs. In series of the compounds $EuLnCuS_3$, the transition into the ordered magnetic state occurs in the narrow temperature range from 2 to 5 K. Compounds, containing Ln^{3+} ions, which magnetic moments are approximately equal to that of Eu^{2+} ion (7.94 μ_B), exhibit ferrimagnetic properties (Table 6). If the magnetic moment of Ln^{3+} ion is lower than that of Eu^{2+} ion, the compound containing Ln^{3+} is ferromagnetic.

3.5. Vibrational properties

The wavenumbers and types of phonon modes were determined by the ab initio calculations. The results for the infrared active modes are given in Tables S4–S5 and Fig. S7. The stoichiometric approximation for the $EuPrCuS_3$ allows to reproduce the lattice constants well, but this approximation provides poor agreement between the calculated IR spectrum and experimental data. The calculated wavenumbers of the IR modes for the $EuPrCuS_3$ are not shown in Fig. S7.

On the basis of the analysis of displacement vectors obtained from the ab initio calculations, the degree of participation of each ion in a particular mode is estimated. The ions being significantly shifted in the mode are listed in the column “Participants” of Tables S4 and S5. The “S” index designates strong shift (“Strong”), “W” designates weak shift (“Weak”). The maximum displacement of ions reaches 0.03–0.04 Å. If displacement is higher than or equal to 0.02 Å, it is indicated as “S”. If the displacement does not exceed 0.01 Å, it is indicated as “W”, and if the displacement is lower than 0.005 Å, then the ion is not mentioned in the column “Participants”. This information is given for crystals $EuGdCuS_3$ (*Pnma*) and $EuYbCuS_3$ (*Cmcm*) in the column "Participants". The calculated values of the ion displacement in the modes are shown in Figs. S8 and S9.

The information of displacements of ions in the modes shows how much an ion is involved in the mode. In series $EuLnCuS_3$ (Ln = Sm-Er), S.G. *Pnma*, europium ions are appreciably involved in the low-wavenumber modes with wavenumbers up to 160 cm^{-1}, as well as the Ln ion. The greatest involvement of europium in IR modes is predicted for the low-wavenumber mode at ~60 cm^{-1} (B_{1u}). The greatest involvement of Ln^{3+} ion in IR modes is predicted for the low-wavenumber mode at ~75–80 cm^{-1} (B_{2u}). The vibrations of copper are found in the IR modes with wavenumbers up to 130 cm^{-1}. The greatest involvement of copper is at the row of IR modes with wavenumbers about 100 cm^{-1}. Sulfur is involved in all IR modes. Sulfur ions S1, S2 and S3 are strongly involved in the IR modes with wavenumbers ~200, ~220 and ~250 cm^{-1}. Both ions S1 and S2 are involved in an intense mode B3u at ~200 cm^{-1}.

In series $EuLnCuS_3$ (Ln = Tm, Yb, Lu), S.G. *Cmcm*, europium ions are appreciably involved in low-wavenumber modes with wavenumbers up to ~130 cm^{-1}, while the Ln ion – up to ~140 cm^{-1}. The highest involvement of europium in IR modes is predicted for the low-wavenumber and low-intense modes at ~ 52–55 cm^{-1} (B_{1u}), ~72–81 cm^{-1} (B_{2u}) and 125 cm^{-1} (B_{3u}). The highest participation of Ln^{3+} ion in IR modes is predicted for the same modes at ~ 52–55 cm^{-1} (B_{1u}) and ~ 72–81 cm^{-1} (B_{2u}). In addition, Ln^{3+} ions are strongly involved in modes at ~ 91–98 cm^{-1} (B_{1u}) and ~ 135–138 cm^{-1} (B_{3u}). The vibrations of copper appear in the IR modes with wavenumbers up to 125 cm^{-1}. The highest involvement of copper in IR modes is predicted for the modes at ~72–81 cm^{-1} (B_{2u}) and at the row of IR modes at about 100 cm^{-1}. Thus, the strong participation of all three ions – Eu, Ln and Cu appears in the low- wavenumber mode at ~72–81 cm^{-1} (B_{2u}). Sulfur is involved in all IR modes. Sulfur is strongly involved in modes with wavenumbers above 180 cm^{-1}. Moreover, S1 ions are most intensely involved. The ion S1 is mainly involved in the IR mode with the maximum wavenumber ~ 300 cm^{-1} (B_{3u}). S1 ions are mainly involved in the two most intense IR modes at ~177–187 cm^{-1} (B_{2u}) and ~200–201 cm^{-1} (B_{1u}). For example, the low-wavenumber IR mode (~72–81 cm^{-1}, B_{2u}) strongly involves three ions (Eu, Ln and Cu), and it is difficult to distinguish the dominant contribution of anyone of them.

The compounds $EuLnCuS_3$ of all the REEs series are transparent for IR radiation in the range of transition wavenumbers 4000–400 cm^{-1} (Fig. S10).

Table 7
Thermal-expansion coefficient for some REEs compounds.

Compound	Temperatures T_{ph} of discontinuous changes α, K	Thermal expansion factor		Fisher's variance ratio
		Temperature range, K	α (T), 1/K	
$EuDyCuS_3$	1072 ± 5	300–1072	$(1.76 \pm 0.03)\cdot10^{-5}$	649
		1072–1280	$(6.07 \pm 0.07)\cdot10^{-5}$	
$EuHoCuS_3$	1135 ± 5	300–1135	$(1.35 \pm 0.02)\cdot10^{-5}$	302
		1135–1280	$(7.47 \pm 0.03)\cdot10^{-5}$	
$EuYbCuS_3$	1195 ± 5	300–1195	$(1.69 \pm 0.02)\cdot10^{-5}$	297
		1195–1280	$(3.73 \pm 0.04)\cdot10^{-4}$	

3.6. Interpretation of dilatometry results

While performing dilatometric analysis of the samples $EuLnCuS_3$ (Ln = La-Nd, Sm, Gd [101], Dy, Ho, Yb, Table 7, Fig. S11) in the temperature range of 900–1200 K, we observed sharp changes (2–3-times/ twice-threefold) of the thermal expansion factor on the constant field extension background. Moreover, the temperature of the discontinuity T_{ph} increases monotonously (Table 7).

The dependence of T_{ph} on ion radii $r\,Ln^{3+}$, where the tetrad effect is apparently observed, is shown in Fig. 3. The experimental points are distinctly described by two straight lines with the parameters determined by the least-squares deviation method. The left line $T_{ph} = a_1 + b_1 r$ indicated the compounds $EuLaCuS_3$, $EuPrCuS_3$, $EuNdCuS_3$ [101] and their regression constrants are equal to $a_1 = -3236 \pm 35$ K, $b_1 = 4267 \pm 34$ K/Å (correlation index is $R_1 = 0.995$). The right line $T_{ph} = a_2 + b_2 r$ indicated the compounds $EuSmCuS_3$ [101], $EuGdCuS_3$ [101], $EuDyCuS_3$, $EuHoCuS_3$, $EuYbCuS_3$ and their regression constrants are equal to $a_2 = 3273 \pm 24$ K, $b_2 = -2392 \pm 32$ K/Å (correlation index is $R_2 = 0.987$).

The discontinuous change of $\alpha(T)$, as observed in our experiments, can be associated with neither high temperature polymorphous transitions, taking place at much higher temperatures

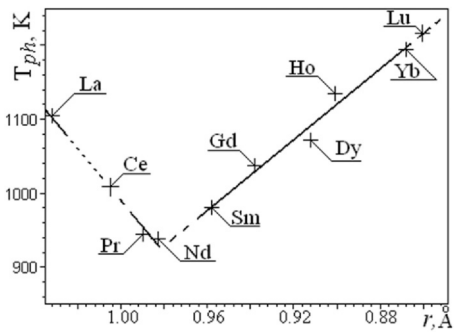

Fig. 3. Dependence T_{ph} on the ion radii of the lanthanoids $r\,Ln^{3+}$.

Table 8
Temperatures of the expected structural transitions.

Compound	$EuCeCuS_3$	$EuTbCuS_3$	$EuErCuS_3$	$EuTmCuS_3$	$EuLuCuS_3$
Ion radii *r*, Å	1.010	0.923	0.890	0.880	0.861
T_{ph}, K	1025 ± 70	1065 ± 50	1144 ± 50	1168 ± 50	1213 ± 50

1437–1594 K nor even more with the compound melting (1539–1738 K) or oxidation, as the analysis was performed in the inert atmosphere. Besides, neither melting nor oxidation were not registered by the DSC method, which, as mentioned above, was used in the analysis process. Fracturing of the sample wasn't observed as well. The discontinuous change of the thermal expansion coefficient is known to be a characteristic feature of the second type phase transition [102]. Therefore, we suppose that, in the samples being examined, in the indicated temperature range the structural transitions take place. With the use of the regression constrants *a* and *b*, it is possible to predict the transition temperatures T_{ph} for other compounds $EuLnCuS_3$ (Ln = Ce, Tb, Er, Tm, Lu), which were not investigated in the dilatometric experiment (Table 8).

For the compounds $EuPrCuS_3$ and $EuNdCuS_3$, the presence of such transitions is confirmed by the XRS results [63]: $EuPrCuS_3$ (ST $BaLaCuS_3$) $\overset{1151\pm5K}{\leftrightarrow}$ $EuPrCuS_3$ (ST Ba_2MnS_3), $EuNdCuS_3$ (ST Eu_2CuS_3) $\overset{939\pm11K}{\leftrightarrow}$ $EuNdCuS_3$ (ST $BaLaCuS_3$) $\overset{1117\pm8K}{\leftrightarrow}$ $EuNdCuS_3$ (ST Ba_2MnS_3). According to the XRS data for $EuCeCuS_3$, the phase transition takes place in the temperature range of 970–1170 K (CT $BaLaCuS_3$) ↔ (CT Ba_2MnS_3) [63], and expected temperature values are in the indicated temperature range (Table 8, Fig. 3). As regarding to some other compounds $EuLnCuS_3$ (Ln = Sm - Lu) in the temperature range from 900 to 1300 K, the presence of the structural transitions has not been confirmed yet by XRS method, so our research will be moving forward.

3.7. Symmetry prediction

In series $A^{2+}LnCuS_3$ (A = Eu, Sr, Pb, Ba), as the radius of divalent metal increases 1.2 Å (rEu^{2+}) < 1.21 Å (rSr^{2+}) < 1.23 Å (rPb^{2+}) < 1.35 Å (rBa^{2+}), gradual decrease of the number of compounds crystallized in ST Ba_2MnS_3 (space group *Pnma*): $EuLnCuS_3$ (Ln = La, Ce, Pr, Nd) → $SrLnCuS_3$ (Ln = La, Ce) → $PbLaCuS_3$ is observed (Table S1, Fig. 4). Proximity of the ion radii of europium/strontium/plumbum to/with REEs results in disorder of the A and Ln atoms in two crystallographic positions that is typical for ST Ba_2MnS_3. Ba radius is much larger than those of light REEs, and, hence, each atom takes independent crystallographic positions, and the compounds crystallize in ST $BaLaCuS_3$. As the radius rA^{2+} increases, the number of compounds crystallized in space group *Cmcm* also increases and A^{2+} ions transform faster into six-coordinated ones.

Since the compound structures of $A^{2+}LnCuS_3$ (A = Eu, Sr, Pb, Ba) are described by 3D and 2D layers of $LnCuS_3$ with A^{2+} ions between them, and polyhedra CuS_4, $AS_7(AS_6)$, LnS_7 (LnS_6) are jointed edge to edge [25,28–30,57,63], the crystal structure deformation and space group changes are dependent on the ion radii rA^{2+}, rLn^{3+} and rCu^{+}. In [26], for the determination of limits of the space groups *Cmcm* and *Pnma* occurring in quaternary chalcogenides the dimensionless factor $t = IR(A)\cdot IR(C)/IR(B)^2$ was suggested. The critical value t = 0.908 governs the boundary line between space groups *Cmcm* and *Pnma*. However, the calculation was based on the experimental data concerning only the field of the space group change in the compounds $ALnCuS_3$ (A = Pb, Ba), and we made an assumption of the necessity for refinement of the structures $PbLnCuS_3$ (Ln = Tb, Dy, Y) [26]. In the contributions [31,33], it was mentioned that the samples of the $PbLnCuS_3$ (Ln = Tb, Dy,Tm, Y) compounds were multi-phase and, besides the main phase, they contained $LnCuS_2$ and PbS. Therefore, the patterns have a lot of small impurity peaks and weak superstructural peaks, which distinguish *Pnma* phase from *Cmcm*, can be overlooked. For this reason, in the present work, we carried out the calculations of t-factor resulted from the complete experimental data on the structures of the compounds $A^{2+}LnCuS_3$ (A = Eu, Sr, Ba) [26–28,30,35,40,42,44,49,50,57,63–68], that allows to predict interphase space group change in the $PbLnCuS_3$ compounds. For this purpose we suggest to use enhanced dependence t'= t + a, where a is a variable parameter. As a result, the formula can be transformed to be $t' = IR(A)\cdot IR(C) + a \times IR(B)^2$, and, thus, the coefficient is as precise as *a* = –0.6. The critical value t' = 0.28 determines limiting date line between orthorhombic space groups *Cmcm* and *Pnma* (Fig. 4).

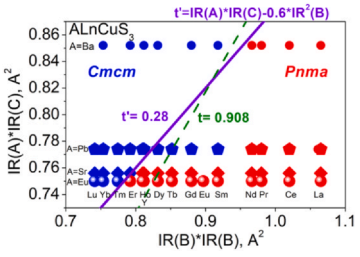

Fig. 4. Phase diagram of the compounds $ALnCuS_3$ in coordinates $IR(B)^2$, IR(A)×IR(C). Critical value of a new tolerance-factor t' = 0.28 fixes limiting date line between space groups *Cmcm* and *Pnma*. The dependence is calculated for the compounds $ALnCuS_3$ (A = Ba, Sr, Eu), while the compounds $PbLnCuS_3$ are given solely for the evaluation. Dashed limiting date line based on the previous formula for the tolerance-factor t [26] is additionally shown. It is obvious that it describes demarcation less distinctly.

As it is seen in Fig. (4), this new formula for the tolerance-factor describes the demarcation line between phase fields for the compounds $ALnCuS_3$ (A = Ba, Sr, Eu), while many compounds $PbLnCuS_3$ (Ln = Tb, Gd, Sm) can not be correctly classified by means of neither t, nor t' tolerance-factors. For these compounds, the dependences assume the existence of *Pnma* phases; however, there is a mention in the literature of *Cmcm* phases only. It should be noted that the *Cmcm* phase can be easily confused with *Pnma* using only X-ray data as a tool, since the difference is only in the presence of weak superstructural peaks.

Our data allowed to detect abnormity in behavior of the three compounds $PbLnCuS_3$ (Ln = Tb, Gd, Sm), and hence, for the last of these, it is necessary to carry out thorough analyses of symmetry using all kinds of experimental techniques. If the *Cmcm* symmetry will be confirmed, then more detailed study of factors resulting in this characteristic feature may be conducted to reach a clear understanding.

4. Conclusions

Generally, ab initio calculations of the structure and dynamics of crystal lattice allow to determine the types of IR modes and assess the degree of the ion participation in each mode. The elastic constants of $EuLnCuS_3$, as the experimental data on those crystals are not available in the literature, were also obtained by calculations. Considerable difference of elastic constants for the compounds $EuLnCuS_3$ (Ln = Sm-Er) and $EuLnCuS_3$ (Ln = Tm, Yb, Lu) was shown. In series of the compounds $EuLnCuS_3$, the transition into ferro- or ferrimagnetic states takes place in the narrow temperature range from 2 to 5 K. The effect of the decrease of the radius of the rare-earth ion and crystallochemical contraction on the properties of compounds is shown. The regularities of changes in the temperatures of phase transformations, relative elongation, and

microhardness of the compounds in the $EuLnCuS_3$ series were determined. The tolerance-factor t' = IR(A)·IR(C) + a × $IR(B)^2$ for the prediction of the structural types of the compounds $ALnCuS_3$ was verified.

Supporting information

Structural types and space groups of the compounds $ALnCuS_3$ (A = Ln = La-Lu), Elastic constants of $EuLnCuS_3$, Bulk modulus, Young's and shear modulus of $EuLnCuS_3$, Calculated IR wavenumbers and mode intensities in $EuLnCuS_3$ (Ln = Sm, Gd-Lu). Polycrystalline samples of the $EuLnCuS_3$ (Ln = La-Lu) compounds, SEM micrographs of $EuLnCuS_3$ samples, Coordination of Eu and Ln in the compounds $EuLnCuS_3$, Dependence of the Young's modulus on the direction in the crystal, Thermal curves for samples of $EuLnCuS_3$ (Ln = Sm, Tm, Yb, Lu), Temperature dependence of the inverse magnetic susceptibility of the compounds $EuLnCuS_3$ for Ln = La, Ce, Pr, Nd, Sm, Ho), Infrared spectra of the compounds, Displacements of ions at phonon modes at $EuLnCuS_3$ (Ln = Gd, Yb) with taking into account all the modes - IR, Raman and "silent", IR-Fourier spectra of the $EuLnCuS_3$ compounds, Temperature dependencies of relative elongation of $EuLnCuS_3$.

CRediT authorship contribution statement

Anna V. Ruseikina: Conceptualization; Thermal, dilatometric, and durometric measurements and their interpretation; Determination of regularities of the of phase transformation temperature changes, percent elongation, and microhardness; Discussion of the phase symmetry predictions; Writing the manuscript; Corresponding author. **Vladimir A. Chernyshev:** Conceptualization, Accomplishment of the DFT calculations, Paper writing. **Dmitriy A. Velikanov:** Magnetic measurements. **Aleksandr S. Aleksandrovsky:** Analysis of results and writing the manuscript. **Nikolay P. Shestakov:** Measurement of IR absorption. **Maxim S. Molokeev:** Participation in the discussion concerned with the phase symmetry prediction, Paper writing. **Maxim V. Grigoriev:** Sulfide samples synthesis, Sample preparation for magnetic, Thermal metering, dilatometry, Participation in the discussion concerned with the phase symmetry prediction. **Oleg V. Andreev:** Consultations on thermal dependencies of sulfides. **Alexander A. Garmonov:** Interpretation of magnetic properties, Paper writing. **Alexey V. Matigorov:** SEM measurements. **Ludmila V. Melnikova:** Paper writing, Linguistic and editorial revision. **Anatoliy A. Kislitsyn:** Interpretation of the dilatometric analysis results, paper writing. **Svetlana S.Volkova:** IR measurements and their interpretation.

Declaration of Competing Interest

The authors declare that they have no known competing financial interests or personal relationships that could have appeared to influence the work reported in this paper.

Acknowledgments

The work was supported by the Ministry of Science and Higher Education of the Russian Federation under Project No. FEUZ-2020-0054; by the "YMNIK" program research project No. 14977GY/2019; by the Ministry of Science and Higher Education of the Russian Federation under project RFMEFI59420X0019.

The use of the equipment of Krasnoyarsk Regional Center of Research Equipment of Federal Research Center "Krasnoyarsk Science Center SB RAS" is acknowledged. A part of measurements was performed in the Research Resource Center "Natural Resource Management and Physico-Chemical Research". The authors would like to thank the staff of the Engineering Center of the Tyumen State University for their help in carrying out physical and chemical tests.

Appendix A. Supporting information

Supplementary data associated with this article can be found in the online version at doi:10.1016/j.jallcom.2021.159968.

References

[1] F.Q. Huang, K. Mitchell, J.A. Ibers, New layered materials: syntheses, structures, and optical and magnetic properties of $CsGdZnSe_3$, $CsZrCuSe_3$, $CsUCuSe_3$, and $BaGdCuSe_3$, Inorg. Chem. 40 (2001) 5123–5126, https://doi.org/10.1021/ic0104353

[2] L.D. Gulay, M. Daszkiewicz, V. Ya Shemet, A. Pietraszko, Crystal structure of the R_2PbS_4 (R = Yb and Lu) compounds, J. Alloy. Comp. 453 (2008) 143–146, https://doi.org/10.1016/j.jallcom.2006.11.110

[3] Y. L, X.-D. Song, R.-C. Zhang, F.-Yi Zhou, J.-W. Zhang, X.-M. Jiang, M. Ji, Y.-L. An, Solvothermal syntheses and characterizations of four quaternary copper sulfides $BaCu_3MS_4$ (M = In, Ga) and $BaCu_2MS_4$ (M = Sn, Ge), Inorg. Chem. 58 (2019) 15101–15109, https://doi.org/10.1021/acs.inorgchem.9b01742

[4] V.P. Sachanyuk, O.V. Parasyuk, A.O. Fedorchuk, V.V. Atuchin, N.V. Pervukhina, A.E. Plotnikov, The system Ag_2Se–Ho_2Se_3 in the 0–50 mol.% Ho_2Se_3 range and the crystal structure of two polymorphic forms of $AgHoSe_2$, Mater. Res. Bull. 42 (2007) 1091–1098, https://doi.org/10.1016/j.materresbull.2006.09.012

[5] A. Assoud, Y. Shi, Q. Guo, H. Kleinke, Crystal and electronic structure of the new quaternary sulfides $TlLnAg_2S_3$ (Ln = Nd, Sm and Gd), J. Solid State Chem. 256 (2017) 6–9, https://doi.org/10.1016/j.jssc.2017.08.028

[6] F. Edhaim, A. Rothenberger, Rare Earth chalcogels $NaLnSnS_4$ (Ln = Y, Gd, Tb) for selective adsorption of volatile hydrocarbons and gases, Z. Anorg. Allg. Chem. 643 (15) (2017) 953–961, https://doi.org/10.1002/zaac.201700082

[7] M. Batouche, T. Seddik, S. Ugur, G. Ugur, S. Messekine, T.V. Vu, O.Y. Khyzhun, DFT-investigation on anisotropy degree of electronic, optical, and mechanical properties of olivine $ZnRE_2S_4$ (RE = Er, Tm) compounds, Mater. Res. Express 7 (1) (2020) 016305, https://doi.org/10.1088/2053-1591/ab6254

[8] N. Zheng, X. Bu, H. Vu, P. Feng, Open-framework chalcogenides as visible-light photocatalysts for hydrogen generation from water, Angew. Chem. Int. Ed. 44 (2005) 5299–5303, https://doi.org/10.1002/anie.200500346

[9] Z. Zhang, J. Zhang, T. Wu, X. Bu, P. Feng, Three dimensional open framework built from Cu-S icosahedral clusters and its photocatalytic property, J. Am. Chem. Soc. 130 (2008) 15238–15239, https://doi.org/10.1021/ja805449p

[10] T. Wu, Q. Zhang, Y. Hou, L. Wang, C. Mao, S.-T. Zheng, X. Bu, P. Feng, Monocopper doping in Cd-In-S supertetrahedral nanocluster via two-step strategy and enhanced photoelectric response, J. Am. Chem. Soc. 135 (2013) 10250–10253, https://doi.org/10.1021/ja404181c

[11] H.B. Luo, L.T. Ren, W.H. Ning, S.X. Liu, J.L. Liu, X.M. Ren, Robust crystalline hybrid solid with multiple channels showing high anhydrous proton conductivity and a wide performance temperature range, Adv. Mater. 28 (2016) 1663–1667, https://doi.org/10.1002/adma.201504591

[12] H. Lin, H. Chen, Y.-J. Zheng, Y.-K. Chen, J.-S. Yu, L.-M. Wu, $Ba_5Cu_8In_2S_{12}$: a quaternary semiconductor with a unique 3D copper-rich framework and ultralow thermal conductivity, Chem. Commun. 53 (2017) 2590–2593, https://doi.org/10.1039/C6CC09904A

[13] T.V. Vu, A.A. Lavrentyev, B.V. Gabrelian, V.A. Tkach, K.D. Pham, O.V. Marchuk, O.V. Parasyuk, O.Y. Khyzhun, First -principles DFT computation and X-ray spectroscopy study of the electronic band structure and optical constants of Cu_2HgGeS_4, Solid State Sci. 104 (2020) 106287, https://doi.org/10.1016/j.solidstatesciences.2020.106287

[14] O.V. Parasyuk, V.V. Atuchin, Y.E. Romanyuk, L.P. Marushko, L.V. Piskach, I.D. Olekseyuk, S.V. Volkov, V.I. Pekhnyo, The $CuGaSe_2$–$CuInSe_2$–2CdS system and single crystal growth of the γ-phase, J. Cryst. Growth 318 (2011) 332–336, https://doi.org/10.1016/j.jcrysgro.2010.10.150

[15] B.S. Sengar, V. Garg, A. Kumar, V. Awasthi, S. Kumar, V.V. Atuchin, S. Mukherjee, Band alignment of Cd-free (Zn, Mg)O layer with $Cu_2ZnSn(S,Se)_4$ and its effect on the photovoltaic properties, Opt. Mater. 84 (2018) 748–756, https://doi.org/10.1016/j.optmat.2018.08.017

[16] K.A. Kokh, V.V. Atuchin, S.V. Adichtchev, T.A. Gavrilova, A.M. Bakhadur, A.S. Klimov, I.V. Korolkov, N.V. Kuratieva, S. Mukherjee, N.V. Pervukhina, N.V. Surovtsev, Cu_2ZnSnS_4 crystal growth using a $SnCl_2$ based flux, CrystEngComm 23 (2021) 1025–1032, https://doi.org/10.1039/D0CE01264E

[17] I. Repins, M. Contreras, M. Romero, Y. Yan, W. Metzger, J. Li, S. Johnston, B. Egaas, C. DeHart, J. Scharf, Characterization of 19.9%-Efficient CIGS, in: 33rd IEEE Photovoltaic Specialists Conference, San Diego, California, Paper NREL/CP-520-42539, 2008.

[18] M.A. Contreras, K. Ramanathan, J. AbuShama, F. Hasoon, D.L. Young, B. Egaas, R. Noufi, Diode characteristics in state-of-the-art ZnO/CdS/$Cu(In_{1-x}Ga_x)Se_2$ solar cells, Prog. Photovolt. Res. Appl. 13 (2005) 209–216, https://doi.org/10.1002/pip.626

[19] I.L. Repins, B.J. Stanbery, D.L. Young, S.S. Li, W.K. Metzger, C.L. Perkins, W.N. Shafarman, M.E. Beck, L. Chen, V.K. Kapur, D. Tarrant, M.D. Gonzalez, D.G. Jensen, T.J. Anderson, X. Wang, L.L. Kerr, B. Keyes, S. Asher, A. Delahoy, B. Roedern, Comparison of device performance and measured transport parameters in widely varying Cu(In,Ga)(Se,S) solar cells, Prog. Photovolt. Res. Appl. 14 (2006) 25–43, https://doi.org/10.1002/pip.654

[20] S.B. Zhang, S.H. Wei, A. Zunger, H. Katayama-Yoshida, Defect physics of the $CuInSe_2$ chalcopyrite semiconductor, Phys. Rev. B. 57 (1998) 9642–9656, https://doi.org/10.1103/PhysRevB.57.9642

[21] H. Matsushita, T. Maeda, A. Katsui, T. Takizawa, Thermal analysis and synthesis from the melts of Cu-based quaternary compounds Cu–III–IV–VI_4 and Cu_2–II–IV–VI_4 (II = Zn, Cd; III = Ga, In; IV = Ge, Sn; VI = Se), J. Cryst. Growth 208 (2000) 416–422, https://doi.org/10.1016/s0022-0248(99)00468-6

[22] S.-M. Kuo, Y.-M. Chang, I. Chung, J.-I. Jang, B.-H. Her, S.-H. Yang, J.B. Ketterson, M.G. Kanatzidis, K.-F. Hsu, New metal chalcogenides $Ba_4CuGa_5Q_{12}$ (Q = S, Se) displaying strong infrared nonlinear optical response, Chem. Mater. 25 (2013) 2427–2433, https://doi.org/10.1021/cm400311v

[23] L. Nian, J. Huang, K. Wu, Z. Su, Z. Yang, S. Pan, $BaCu_2MIVQ_4$ (MIV = Si, Ge, and Sn; Q = S, Se): synthesis, crystal structures, optical performances and theoretical calculations, RSC Adv. 7 (2017) 29378–29385, https://doi.org/10.1039/c7ra05022d

[24] X.W. Lei, M. Yang, S.Q. Xia, X.C. Liu, M.Y. Pan, X. Li, X.T. Tao, Synthesis, structure and bonding, optical properties of Ba_4MTrQ_6 (M = Cu, Ag; Tr = Ga, In; Q = S, Se), Chem. - Asian J. 9 (2014) 1123–1131, https://doi.org/10.1002/asia.201301495

[25] L.A. Koscielski, J.A. Ibers, The structural chemistry of quaternary chalcogenides of the type AMM'Q_3, Z. Anorg. Allg. Chem. 638 (2012) 2585–2593, https://doi.org/10.1002/zaac.201200301

[26] N.O. Azarapin, A.S. Aleksandrovsky, V.V. Atuchin, T.A. Gavrilova, A.S. Krylov, M.S. Molokeev, Sh Mukherjee, A.S. Oreshonkov, O.V. Andreev, Synthesis, structural and spectroscopic properties of orthorhombic compounds $BaLnCuS_3$ (Ln = Pr, Sm), J. Alloy. Compd. 832 (2020) 153134, https://doi.org/10.1016/j.jallcom.2019.153134

[27] M. Eberle, T. Schleid, Expanding the SrCuRES3 series with the rare-earth metals scandium and yttrium, in: 24th Annual Conference of the German Crystallographic Society, Stuttgart, March 14–17, 2016. https://books.google.ru/books?id=klu7CwAAQBAJ&pg=PT237&dq=SrCuScS (Accessed 19 May 2020).

[28] M. Wakeshima, F. Furuuchi, Y. Hinatsu, Crystal structures and magnetic properties of novel rare-earth copper sulfides, $EuRCuS_3$ (R = Y, Gd-Lu), J. Phys. Condens. Matter 16 (2004) 5503–5518, https://doi.org/10.1088/0953-8984/16/30/012

[29] F. Furuuchi, M. Wakeshima, Y. Hinatsu, Magnetic properties and (151) Eu Mossbauer effects of mixed valence europium copper sulfide Eu_2CuS_3, J. Solid State Chem. 177 (2004) 3853–3858, https://doi.org/10.1016/j.jssc.2004.04.034

[30] A.V. Ruseikina, L.A. Solovyov, V.A Chernyshev, A.S. Aleksandrovsky, O.V. Andreev, S.N. Krylova, A.S. Krylov, D.A Velikanov, M.S. Molokeev, N.G. Maximov, M.V. Grigoriev, A.A. Garmonov, A.V. Matigorov, Synthesis, structure, and properties of $EuErCuS_3$, J. Alloy. Comp. 805 (2019) 779–788, https://doi.org/10.1016/j.jallcom.2019.07.059

[31] L.D. Gulay, V. Ya Shemet, I.D. Olekseyuk, Crystal structures of the compounds $YCuS_2$, Y_3CuSnS_7 and $YCuPbS_3$, J. Alloy. Comp. 388 (2005) 59–64, https://doi.org/10.1016/j.jallcom.2004.06.074

[32] T.D. Brennan, J.A. Ibers, $LaPbCuS_3$: Cu(I) insertion into the α-La_2S_3 framework, J. Solid State Chem. 97 (1992) 377–382, https://doi.org/10.1016/0022-4596(92)90046-X

[33] L.D. Gylay, I.D. Olekseyuk, M. Wolcyrz, J. Stepien-Damm, Crystal structures of the $RCuPbS_3$ (R = Tb, Dy, Ho, Er, Tm, Yb and Lu) compounds, J. Alloy. Comp. 399 (2005) 189–195, https://doi.org/10.1016/j.jallcom.2005.03.036

[34] S.T. Bairamova, M.R. Bagieva, S.M. Agapashaeva, O.M. Aliev, Synthesis and Properties of Structural Analogs of the Mineral Bournonite, Inorg. Mater. 47 (4) (2011) 345–348, https://doi.org/10.1134/S0020168511040054

[35] M.A. Eberle, S. Strobel, T. Schleid, SrCuNdS3: a new compound with two different crystal structures. Jahrestagung der DGK, Berlin, Maerz 17–20, 2014, MS05-48 DUMMY7.

[36] S. Strobel, T. Schleid, Three structure types for strontium copper (I) lanthanide (III) selenides $SrCuMSe_3$ (M = La, Gd, Lu), J. Alloy. Compd. 418 (2006) 80–85.

[37] S. Strobel, T. Schleid, Quaternary strontium copper (I) lanthanoid (III) selenides with cerium and praseodymium: $SrCuCeSe_3$ and $SrCuPrSe_3$, unequal brother and sister, Z. Naturforsch. B 59 (9) (2004) 985–991, https://doi.org/10.1515/znb-2004-0907

[38] S. Maier, J. Prakash, D. Berthebaud, O. Perez, S. Bobev, F. Gascoin, Crystal structures of the four new quaternary copper (I)-selenides $A_{0.5}CuZrSe_3$ and $ACuYSe_3$ (A= Sr, Ba), J. Solid State Chem. 242 (2016) 14–20, https://doi.org/10.1016/j.jssc.2016.06.023

[39] Y. Yang, J.A. Ibers, Synthesis and characterization of a series of quaternary chalcogenides $BaLnMQ_3$ (Ln = rare earth, M = coinage metal, Q = Se or Te), J. Solid State Chem. 147 (1999) 366–371, https://doi.org/10.1006/jssc.1999.8359

[40] P. Wu, A.E. Christuk, J.A. Ibers, New quaternary chalcogenides $BaLnMQ_3$ (Ln = Rare Earth or Sc; M = Cu, Ag; Q=S, Se). Structure and property variation vs rare-Earth element, J. Solid State Chem. 110 (1994) 337–344, https://doi.org/10.1006/jssc.1994.1177

[41] P. Lemoine, D. Carré, M. Guittard, Structure du sulfure d'europium et de cuivre Eu_2CuS_3, Acta Cryst. 42 (1986) 390–391, https://doi.org/10.1107/S0108270186096063

[42] A.E. Christuk, P. Wu, J.A. Ibers, New quaternary chalcogenides $BaLnMQ_3$ (Ln = Rare Earth; M = Cu, Ag; Q = S, Se). Structures and grinding-Induced phase transition in $BaLaCuQ_3$, J. Solid State Chem. 110 (1994) 330–336, https://doi.org/10.1006/jssc.1994.1176

[43] P. Wu, J.A. Ibers, Synthesis of the new quaternary sulfides $K_2Y_4Sn_2S_{11}$ and $BaLnAgS_3$ (Ln = Er, Y, Gd) and the structures of $K_2Y_4Sn_2S_{11}$ and $BaErAgS_3$, J. Solid State Chem. 110 (1994) 156–161, https://doi.org/10.1006/jssc.1994.1150

[44] A.V. Ruseikina, M.S. Molokeev, V.A Chernyshev, A.S. Aleksandrovsky, A.S. Krylov, S.N. Krylova, D.A Velikanov, M.V. Grigoriev, N.G. Maximov, N.P. Shestakov, A.A. Garmonov, A.V. Matigorov, A.S. Tarasov, M.V. Rautskii, N.A Khritokhin, L.V. Melnikova, N.Yu Tretyakov, Synthesis, structure, and properties of $EuScCuS_3$ and $SrScCuS_3$, J. Solid State Chem. 296 (2021) 121926, https://doi.org/10.1016/j.jssc.2020.121926

[45] S.T. Bayramova, S.A. Guliyeva, O.M. Aliyev, The synthesis and physico-chemical properties of quadruple sulphides like $PbLnCuS_3$, Chem. Probl. 2 (2010) 249–252 http://chemprob.org/wp-content/uploads/2018/06/Байрамова-4-4.pdf.

[46] C. Liu, P. Hou, W. Chai, J. Tian, X. Zheng, Y. Shen, M. Zhi, C. Zhou, Y. Liu, Hydrazine-hydrothermal syntheses, characterizations and photoelectrochemical properties of two quaternary chalcogenidoantimonates(III) $BaCuSbQ_3$ (Q = S, Se), J. Alloy. Compd. 679 (2016) 420–425, https://doi.org/10.1002/chin.201630020

[47] N.V. Sikerina, O.V. Andreev, Crystal structures of $SrLnCuS_3$ (Ln= Gd, Lu), Russ. J. Inorg. Chem. 52 (2007) 581–584, https://doi.org/10.1134/S0036023607040183

[48] V.O. Aliev, N.R. Akhmedova, S.M. Agapasheva, O.M. Aliev, Crystal growth and physicochemical properties of structural analogs of krupkaite, Inorg. Mater. 45 (2009) 717–722, https://doi.org/10.1134/s0020168509070024

[49] N.V. Sikerina, Regularities of phase equilibria in SrS-Ln_2S_3-Cu_2S systems, preparation and structure of SrLnCuS3 compounds. PhD Dissertation, University of Tyumen, Tyumen, 2005. https://elib.utmn.ru/jspui/bitstream/ru-tsu/2441/1/472.pdf (Accessed 19 June 2020).

[50] A.V. Solovieva, Regularities of phase equilibria in $A^{II}S$ – FeS, $A^{II}S$ – FeS – Ln_2S_3, $A^{II}S$ – Cu_2S – Ln_2S_3 (A^{II} = Mg, Ca, Sr, Ba; Ln = La – Lu) systems. PhD Dissertation, University of Tyumen, Tyumen, 2012. https://search.rsl.ru/ru/record/01005019099 (Accessed 19 May 2020).

[51] L.D. Gulay, V.Ya Shemet, I.D. Olekseyuk, J. St epie´n-Dammb, A. Pietraszko, L.V. Koldun, J.O. Filimonyuk, Investigation of the R_2S_3-Cu_2S-PbS (R= Y,Dy, Gd, Ho and Er) systems, J. Alloy. Compd. 431 (2007) 77–84, https://doi.org/10.1016/j.jallcom.2006.05.029

[52] R.A. Aliyeva, S.T. Bayramova, O.M. Aliyev, Phase equilibriums in quasi-ternary system PbS–Cu_2S–La_2S_3, Chem. Probl. 3 (2008) 503–508.

[53] S.T. Bayramova, S.I. Aliyeva, D.S. Ajdarova, OM Aliyev, Phase equilibriums in quasi-ternary system Cu_2S-PbS-Gd_2S_3 by sections $CuGdS_2$-PbS and Cu_2S-PbCuGdS_3, Chem. Probl. 4 (2015) 424–427, https://elib.pstu.ru/vufind/EdsRecord/edselr,edselr.26507159.

[54] N.V. Sikerina, A.V. Solov'eva, E.N. Toroshchin, O.V. Andreev, Phase equilibriums in the BaS–Cu_2S–Gd_2S_3 system, Russ. J. Inorg. Chem. 52 (12) (2007) 1982–1986, https://doi.org/10.1134/S0036023607120285

[55] R.A. Aliyeva, S.T. Bayramova, S.M. Agapashaeva, O.M. Aliyev, Phase equilibriums in quasi-ternary system Cu_2S-PbS-Sm_2S_3, in: XIX Mendeleev Congress on General and Applied Chemistry, Volgograd, September 25–30, 2011, p. 467. https://b-ok.cc/book/3152556/859c91 (accessed 19 June 2020).

[56] A.V. Ruseikina, O.V. Andreev, E.O. Galenko, S.I. Koltsov, Trends in thermodynamic parameters of phase transitions of lanthanide sulfides $SrLnCuS_3$ (Ln = La–Lu), J. Therm. Anal. Calorim. 128 (2017) 993–999, https://doi.org/10.1007/s10973-016-6010-9

[57] A.V. Ruseikina, Zh.A. Demchuk, Crystal structure and properties of $AHoCuS_3$ (A = Sr or Eu), Russ. J. Inorg. Chem. 62 (2017) 27–32, https://doi.org/10.1134/S0036023617010168

[58] A.V. Ruseikina, O.V. Andreev, Phase equilibria in systems $DyCuS_2$–EuS and Cu_2S–Dy_2S_3–EuS, Russ. J. Inorg. Chem. 63 (2018) 1494–1500, https://doi.org/10.1134/S0036023618110141

[59] A.V. Ruseikina, O.V. Andreev, Phase equilibria in the Cu_2S-La_2S_3-EuS system, Russ. J. Inorg. Chem. 62 (2017) 610–618, https://doi.org/10.1134/S0036023617050199

[60] O.V. Andreev, A.V. Ruseikina, L.A. Solov'ev, Phase diagrams of sections in the EuS–Cu_2S–Nd_2S_3 system, Russ. J. Inorg. Chem. 56 (2011) 792–797, https://doi.org/10.1134/S0036023611040024

[61] I.E. Grey, H. Steinfink, Crystal structure of Ba_2MnSe_3. Linear antiferromagnetism in Ba_2MnX_3 (X = S,Se), Inorg. Chem. 10 (1971) 691–696, https://doi.org/10.1021/ic50098a007

[62] M.F. Mansuetto, P.M. Keane, J.A. Ibers, Synthesis, structure, and conductivity of the new group IV chalcogenides $KCuZrQ_3$ (Q = S, Se, Te), J. Solid State Chem. 101 (1992) 257–264, https://doi.org/10.1016/0022-4596(92)90182-U

[63] A.V. Ruseikina, O.V. Andreev, Regularities of change in the structural parameters of $EuLnCuS_3$ (Ln = La-Nd, Sm, Gd, Ho), Russ. J. Inorg. Chem. 62 (2017) 160–167, https://doi.org/10.1134/S0036023617020140

[64] A.V. Ruseikina, L.A. Solovyov, M.V. Grigoriev, O.V. Andreev, Crystal structure variations in the series $SrLnCuS_3$ (Ln = La, Pr, Sm, Gd, Er and Lu), Acta Crystallogr. C75 (2019) 584–588, https://doi.org/10.1107/S2053229619004984

[65] A.V. Ruseikina, L.A. Solov'ev, Crystal Structures of α- and β-$SrCeCuS_3$, Russ. J. Inorg. Chem. 61 (2016) 482–487, https://doi.org/10.1134/S0036023616040161

[66] A.V. Ruseikina, M.V. Grigoriev, E.O. Galenko, G.A. Sadykhov, Crystal structure and properties $SrTbCuS_3$, in: XX Mendeleev Congress on general and applied chemistry, Ekaterinburg, September 26–30, 2016.

[67] A.V. Ruseikina, L.A. Solov'ev, E.O. Galenko, M.V. Grigor'ev, Refined crystal structures of $SrLnCuS_3$ (Ln = Er, Yb), Russ. J. Inorg. Chem. 63 (2018) 1225–1231, https://doi.org/10.1134/S0036023618090140

[68] A.V. Ruseikina, E.O. Galenko, M.V. Grigor'ev, G.A. Sadykhov, Structure and properties of $SrTmCuS_3$ compound, in: IX international conference Kinetics and mechanism of crystallization. Crystallization and Materials of the Future, Ivanovo, September 13–16, 2016.

[69] B.F. Dzhurinskii, G.A. Bandurkin, Regularities of lanthanides properties and inorganic materials, Izv. Akad. Nauk SSSR Neorg. Mater. 15 (6) (1979) 1024–1027.

[70] B.F. Dzhurinskii, Regularities of the rare-earth elements properties, Zh. Neorg. Khim. 25 (1980) 79–86.

[71] R.D. Shannon, Revised effective ionic radii and systematic studies of interatomic distances in halides and chalcogenides, Acta Cryst. Sect. A 32 (5) (1976) 751–767 file:///C:/Users/adesc/Downloads/ShannonRevisedIonicRadii1976%20(1).pdf (accessed 2020-06-19).
[72] E.A. Olennikov, Logger complex and processing of the experimental thermal analyses data. Information system of the two-component state system diagram. PhD Dissertation, University of Tyumen, Tyumen, 2003. https://search.rsl.ru/ru/record/01002650234 (Accessed 21 June 2020).
[73] K. Brandenburg, Diamond e visual crystal structure information system crustal impact, Post 1251, D-53002 Boon.
[74] A.G. Kolmakov, V.F. Terentyev, M.B. Bakirov, Hardness Measurement Methods, second ed., Intermet Engineering, Moscow, 2005. http://www.pseudology.org/science/Metody_izmer_tverdosti2.pdf.
[75] D.A. Velikanov, Magnetometer with a superconducting quantum interferometric sensor, RF Pat., 2481591, 2013. http://www.freepatent.ru/patents/2481591 (Accessed 19 October 2020).
[76] D.A. Velikanov, Vibration magnetometer, RF Pat., 2341810, 2008. http://www.freepatent.ru/patents/2341810 (Accessed 19 October 2020).
[77] D.A. Velikanov, High-sensitivity measurements of the magnetic properties of materials at cryogenic temperatures, Inorg. Mater. Appl. Res. 11 (4) (2020) 801–808, https://doi.org/10.1134/S2075113320040413
[78] E.N. L'vovskii, Statisticheskie metody postroeniya empiricheskikh formul (Statistical Methods of Deriving Empirical Formulas), Vysshaya Shkola, Moscow, 1988.
[79] V.G. Tsirelson, Quantum chemistry. Molecules, molecular systems and solids, third ed., Binom. KnowledgeLab, Moscow, 2014.
[80] A.D. Becke, Density-functional thermochemistry. III. The role of exact exchange, J. Chem. Phys. 98 (1993) 5648–5652, https://doi.org/10.1063/1.464913
[81] P.L. Stephens, F.J. Devlin, C.F. Chabalowski, M.J. Frisch, Ab Initio calculation of vibrational absorption and circular dichroism spectra using density functional force fields, J. Phys. Chem. 98 (1994) 11623–11627, https://doi.org/10.1021/j100096a001
[82] V.V. Atuchin, V.V. Kaichev, I.V. Korolkov, A.A. Saraev, I.B. Troitskaia, T.V. Perevalov, V.A. Gritsenko, Electronic structure of noncentrosymmetric α-GeO_2 with oxygen vacancy: ab initio calculations and comparison with experiment, J. Phys. Chem. C 118 (2014) 3644–3650, https://doi.org/10.1021/jp411751c
[83] Y.N. Zhuravlev, V.V. Atuchin, Comprehensive density functional theory studies of vibrational spectra of carbonates, Nanomaterials 10 (2020) 2275, https://doi.org/10.3390/nano10112275
[84] R. Dovesi, V.R. Saunders, C. Roetti, R. Orlando, C.M. Zicovich-Wilson, F. Pascale, B. Civalleri, K. Doll, N.M. Harrison, I.J. Bush, P. D'Arco, M. Llunel, M. Causa , Y. Noel, L. Maschio, A. Erba, M. Rerat, S. Casassa, CRYSTAL17 User's Manual, 2018. http://www.crystal.unito.it/Manuals/crystal17.pdf.
[85] Crystal . http://www.crystal.unito.it/index.php (Accessed 31 July 2019).
[86] M. Dolg, H. Stoll, A. Savin, H. Preuss, Energy-adjusted pseudopotentials for the rare earth elements, Theor. Chim. Acta 75 (1989) 173–194, https://doi.org/10.1007/BF00528565
[87] M. Dolg, H. Stoll, H. Preuss, A combination of quasi relativistic pseudopotential and ligand field calculations for lanthanoid compounds, Theor. Chim. Acta 85 (1993) 441–450, https://doi.org/10.1007/BF01112983
[88] Energy-consistent Pseudopotentials of the Stuttgart/Cologne Group. http://www.tc.uni-koeln.de/PP/clickpse.en.html (Accessed 29 October 2018).
[89] Doll, N.M. Harrison, Chlorine adsorption on the Cu(111) surface, Chem. Phys. Lett. 317 (2000) 282–289, https://doi.org/10.1016/S0009-2614(99)01362-7
[90] T. Ouazzani, A. Lichanot, C. Pisani, C. Roetti, Relaxation and electronic structure of surfaces in lithium sulphide: a Hartree-Fockab initio approach, J. Phys. Chem. Solids 54 (1993) 1603–1611, https://doi.org/10.1016/0022-3697(93)90356-V
[91] M. Dolg, H. Stoll, A. Savin, H. Preuss, Energy-adjusted pseudopotentials for the rare earth elements, Theor. Chim. Acta 75 (1989) 173–194, https://doi.org/10.1007/BF00528565
[92] M. Dolg, H. Stoll, H. Preuss, A combination of quasirelativistic pseudopotential and ligand field calculations for lanthanoid compounds, Theor. Chim. Acta 85 (1993) 441–450, https://doi.org/10.1007/BF01112983
[93] J. Yang, M. Dolg, Valence basis sets for lanthanide 4f-in-core pseudopotentials adapted for crystal orbital ab initio calculations, Theor. Chem. Acc. 113 (4) (2005) 212–224, https://doi.org/10.1007/s00214-005-0629-0
[94] A. Weigand, X. Cao, J. Yang, M. Dolg, Quasirelativistic f-in-core pseudopotentials and core-polarization potentials for trivalent actinides and lanthanides: molecular test for trifluorides, Theor. Chem. Acc. 126 (2010) 117–127, https://doi.org/10.1007/s00214-009-0584-2
[95] V.A. Chernyshev, A.E. Nikiforov, V.P. Petrov, A.V. Serdtsev, M.A. Kaschenko, S.A. Klimin, Structure and lattice dynamics of rare-earth ferroborate crystals: ab initio calculation, Phys. Solid State 58 (2016) 1642–1650, https://doi.org/10.1134/S1063783416080096
[96] V.A. Chernyshev, V.P. Petrov, A.E. Nikiforov, Lattice dynamics of rare-earth titanates with the structure of pyrochlore $R_2Ti_2O_7$ (R = Gd, Tb, Dy, Ho, Er, Tm, Yb, and Lu): ab initio calculation, Phys. Solid State 57 (2015) 996–1002, https://doi.org/10.1134/S1063783415050078
[97] Y. Tian, B. Xu, Z. Zhao, Microscopic theory of hardness and design of novel superhard crystals, Int. J. Refract. Met. Hard Mater. 33 (2012) 93–106, https://doi.org/10.1016/j.ijrmhm.2012.02.021 accessed 2020-06-19.
[98] A.V. Ruseikina, O.V. Andreev, Synthesis of compounds $EuLnCuS_3$ (Ln"La-Nd), Temperature and heat of fusion, Vestn. Tyumensk. Gos. Univ. 3 (2010) 221–227 https://www.elibrary.ru/item.asp?id=15518992.
[99] A.V. Ruseikina, Zh.A. Demtchuk, AA Kislicyn, Warmth of phase transformations connection of $EuGdCuS_3$, Vestn. Tyumensk. Gos. Univ. 5 (2012) 19–25, https://www.elibrary.ru/item.asp?id=17755886.
[100] M. Husain, A. Batra, K.S. Srivastava, Electonegative, radii elements, Polyhedron 8 (9) (1989) 1233–1234.
[101] Yu.A. Murashko, A.V. Ruseikina, A.A. Kislitsyn, O.V. Andreev, Optical and thermal properties of the $EuLnCuS_3$ (Ln = La, Pr, Sm, Gd), Inorg. Mater. 51 (2015) 1213–1218, https://doi.org/10.1134/S0020168515120079
[102] L.D. Landau, E.M. Lifshits, Theoretical Physics. Statistical Mechanics, Nauka, Moscow, 1964.